

# Nonthermal Emission from Accreting and Merging Clusters of Galaxies

Yutaka Fujita<sup>1</sup>

*National Astronomical Observatory, Osawa 2-21-1, Mitaka, Tokyo 181-8588, Japan*

yfujita@th.nao.ac.jp

and

Craig L. Sarazin

*Department of Astronomy, University of Virginia, P.O. Box 3818, Charlottesville, VA 22903-0818*

sarazin@virginia.edu

## ABSTRACT

We compare the nonthermal emission from clusters of galaxies undergoing minor mergers (“accreting” clusters) and major mergers (“merging” clusters). We define major mergers as the mergers that change the inner dark matter structure of clusters; minor mergers are all others. For accreting clusters, the radial distribution of the nonthermal emission in the clusters is also calculated. The relativistic electrons, which are the origin of the nonthermal radiation through inverse Compton (IC) and synchrotron emission, are assumed to be accelerated at shocks produced by accretion or mergers. We estimate the typical accretion rate and merger probability according to a hierarchical clustering model. We predict that in the inner region of accreting clusters the nonthermal emission has a flat spatial distribution at all frequency. For synchrotron and hard X-ray emissions, we predict an increase of the emissions at the cluster edge due to accretion. We show that the total luminosity of IC emission from accreting and merging clusters are similar. On the other hand, the luminosity of synchrotron radio emission of

---

<sup>1</sup>Present address: Department of Astronomy, University of Virginia, P.O. Box 3818, Charlottesville, VA 22903-0818

the former is much smaller than that of the latter. We show that about 10% of clusters at  $z \sim 0$  should have hard X-ray and radio nonthermal emissions due to their last major merger, which are comparable to or dominate those due to ongoing accretion. Moreover, 20 – 40% of clusters should have significant EUV emission due to their last merger. We also investigate the case where the criterion of mergers is relaxed. If we extend the definition of a merger to an increase in the mass of the larger subcluster by at least 10% of its initial mass, about 20 – 30% of clusters at  $z \sim 0$  should have hard X-ray and radio nonthermal emissions due to the merger even in a low density universe. We compare the results with observations. We find that the observed EUV emission from clusters is not attributed to accretion. If the diffuse radio emission observed in clusters is synchrotron emission from electrons accelerated via accretion or merging, the magnetic fields of clusters are generally as small as  $\sim 0.1 \mu\text{G}$ . One concern is that this is a significantly weaker field than that implied by Faraday rotation measurements.

*Subject headings:* cosmic rays—galaxies: clusters: general—intergalactic medium—radiation mechanism: nonthermal—ultraviolet: general—X-rays: general

## 1. Introduction

Clusters of galaxies are luminous, extended X-ray sources. The bulk of this radiation is thermal emission (mainly thermal bremsstrahlung and line emission) from hot gas with temperatures of  $\sim 7$  keV (the intracluster medium or ICM). On the other hand, recent observations at very soft X-ray/extreme ultraviolet (EUV) energies ( $\sim 0.1$  keV) and at very hard X-ray energies ( $\sim 20$  keV) suggest excess emission beyond that expected from the thermal ICM emission.

Extreme ultraviolet (EUV) or very soft X-ray excess emissions have been detected from a number of clusters (Lieu et al. 1996a,b; Bowyer, Lampton, & Lieu 1996; Bowyer & Berghöfer 1998; Mittaz, Lieu, & Lockman 1998; Kaastra et al. 1999; Lieu, Bonamente, & Mittaz 1999; Lieu et al. 1999; Berghöfer, Bowyer, & Korpela 2000a; Bonamente, Lieu, & Mittaz 2001). Although the properties and even the existence of this EUV emission is still controversial (Arabadjis & Bregman 1999; Bowyer, Berghöfer, & Korpela 1999; Berghöfer, Bowyer, & Korpela 2000b), one hypothesis is that it is the inverse Compton (IC) scattering of cosmic microwave background (CMB) photons by relativistic electrons (Hwang 1997; Bowyer & Berghöfer 1998; Enßlin & Biermann 1998; Sarazin & Lieu 1998). These electrons would have energies of  $E = \gamma m_e c^2 \sim 150$  MeV and Lorentz factors  $\gamma \sim 300$ .

Hard X-ray emission in excess of the thermal emission and detected as a nonthermal tail at energies  $\gtrsim 20$  keV has been seen in at least two clusters. The Coma cluster was detected with both *BeppoSAX* (Fusco-Femiano et al. 1999) and the *Rossi X-Ray Timing Explorer* (*RXTE*; Rephaeli, Gruber, & Blanco 1999). *BeppoSAX* also has detected Abell 2256 (Fusco-Femiano et al. 2000). Possible weaker excesses may have been seen in Abell 2199 (Kaastra et al. 1999) and Abell 3667 (Fusco-Femiano et al. 2001). Again, this radiation is believed to be IC emission, in this case produced by relativistic electrons with  $E = \gamma m_e c^2 \sim 5$  GeV and Lorentz factors  $\gamma \sim 10^4$ .

A number of clusters are known to have diffuse radio sources (e.g., Kim et al. 1990; Giovannini et al. 1993; Giovannini & Feretti 2000; Kempner & Sarazin 2001). These radio sources have very steeply declining radio spectra, and are not associated with individual galaxies. They are referred to as radio halos when they appear projected on the center of the cluster, and are called relics when they are found on the cluster periphery (although they have other distinctive properties). The origin of the radio emission is definitely nonthermal, being synchrotron emission produced by relativistic electrons radiating in the intracluster magnetic fields. The typical energy of the electrons which produce the radio emission depends on the observed frequency and on the intracluster field, but is estimated to be several GeV; thus, basically the same electrons which produce the IC hard X-ray emission produce this diffuse radio emission

The relativistic electrons are often believed to be accelerated by shocks in ICM (Jaffe 1977; Roland 1981; Schlickeiser, Sievers, & Thiemann 1987), although alternative origins are possible (Atoyan & Völk 2000; Enßlin & Gopal-Krishna 2001). These shocks may be attributed to the interaction between jets originated from active galactic nuclei (AGNs) and ICM. On the other hand, given the large size of the the diffuse radio relics and halos and the extent of EUV/soft X-ray emission in clusters, it may be easier to understand these sources if the particles are produced by mergers between clusters (Roettiger, Burns, & Stone 1999). Takizawa & Naito (2000) calculated the nonthermal emission from relativistic electrons accelerated around the shocks produced during a merger of clusters with equal mass. They found that the hard X-ray and radio emissions are luminous only while signatures of merging events are clearly seen in the ICM. On the other hand, EUV emission is still luminous after the system has relaxed.

In this paper, we will divide cluster mergers into two groups: mergers that lead to a mass increase by as much as the initial mass of main subcluster and to the reconstruction of cluster dark matter structure, and the mergers of smaller subclusters into a much larger main cluster. We refer to the former process as a “merger,” and the latter as “accretion”. Kauffmann & White (1993) indicated that the percentage of clusters undergoing merging

events with roughly equal-mass progenitors over a 1 Gyr period at low redshift is 3-15 percent. Thus the results of Takizawa & Naito (2000) can be compared with the observations of only a small fraction of clusters. On the other hand, Kauffmann & White (1993) showed that most clusters are accreting smaller clumps at present. Through this accretion, shocks form around the virial radius of clusters (Evrard, Metzler, & Navarro 1996; Takizawa & Mineshige 1998; Eke, Navarro, & Frenk 1998; Miniati et al. 2000). Kang, Rachen, & Biermann (1997) modeled the acceleration of very high energy particles around the shock at the cluster edge. Nonthermal emission may be produced by the accelerated electrons at the cluster accretion shock, although the number of such electrons and the emission power may be small compared with the case of violent mergers. In the future, it may be possible to observe fainter nonthermal emission from clusters, and to study the nonthermal radiation from large samples of clusters statistically. Thus, it would be important to study the nonthermal emission not only from rare clusters undergoing violent merging events but also that from normal clusters undergoing accretion.

In this paper, we study the nonthermal emission from accreting clusters and compare the results with the emission from clusters undergoing major mergers. Sarazin (1999) considered a simple model for the time evolution of the relativistic electrons and nonthermal emission from clusters accreting ambient medium, based on the self-similar accretion solution of Bertschinger (1985). However, this paper did not directly compare the expected fluxes of merging and accreting clusters, as we do here. Enßlin et al. (1998) proposed that the shocks caused by accretion onto clusters and the resulting acceleration of electrons in the shocks are responsible for observed cluster radio relics using the results of one dimensional simulations of cluster formation in the Einstein-de Sitter universe. However, they mainly focused on the emission of individual radio relics and did not consider EUV and hard X-ray emissions. We consider EUV, hard X-ray and radio emissions from clusters undergoing accretion or merger generally. The somewhat arbitrary distinction between accretion and major mergers may be useful, because they differ considerably in the the power and spatial distribution of the resultant nonthermal emission. For example, while there is evidence that the strongest radio halos appear only in those clusters currently experiencing major mergers (e.g., Buote 2001), many other clusters may have weaker diffuse radio emission, below the sensitivity of current surveys, which is associated with weaker mergers (accretion). This paper is organized as follows: § 2, we summarize our models. We give the results of our calculations in § 3, and compare them with observations in § 4. Conclusions are given in § 5.

## 2. Models

### 2.1. Mass Evolution of a Cluster

In order to follow the evolution of clusters or, more generally, ‘dark halos,’ we use a modification of an extended Press & Schechter model derived by Salvador-Sole, Solanes, & Manrique (1998). From now on, we call the model the SSM model. In this model, major mergers among clusters and continuous accretion are distinguished. Here, major mergers mean the mergers that change the core structure of dark halos; minor mergers are all others. We will refer to major mergers as ‘mergers’, and will use the term ‘accretion’ to describe the cumulative effect of minor mergers. Note that a ‘merger’ does not necessary mean a binary merger; it also includes multiple mergers. The details of the model are also described in Enoki, Takahara, & Fujita (2001).

In this model, the mass function of dark halos is given by the Press & Schechter (PS) mass function;

$$n(M, t) dM = \sqrt{\frac{2}{\pi}} \frac{\rho_0}{M} \frac{\delta_c(t)}{\sigma^2(M)} \left| \frac{d\sigma(M)}{dM} \right| \exp \left[ -\frac{1}{2} \frac{\delta_c^2(t)}{\sigma^2(M)} \right] dM, \quad (1)$$

where  $n(M, t) dM$  gives the number density of clusters with masses in the range  $M \rightarrow M + dM$  per comoving volume. Here,  $\rho_0$  is the present mean density of the universe,  $\delta_c(t)$  is the critical density contrast for collapse at  $t$ , and  $\sigma(M)$  is the rms density fluctuation in spheres containing a mean mass  $M$  (Press & Schechter 1974). In this paper, we use an approximate formula of  $\delta_c(t)$  for spatially flat cosmological model (Nakamura & Suto 1997) and a fitting formula of  $\sigma(M)$  for the CDM fluctuation spectrum (Kitayama 1997).

Lacey & Cole (1993) obtained the instantaneous merger rate for halos with mass  $M$  at time  $t$  per infinitesimal range of final mass  $M' > M$ ; it is given by

$$\begin{aligned} r_{\text{LC}}^m(M \rightarrow M', t) dM' &\equiv \sqrt{\frac{2}{\pi}} \left| \frac{d\delta_c(t)}{dt} \right| \frac{1}{\sigma^2(M')} \left| \frac{d\sigma(M')}{dM'} \right| \\ &\times \left[ 1 - \frac{\sigma^2(M')}{\sigma^2(M)} \right]^{-3/2} \\ &\times \exp \left\{ -\frac{\delta_c^2(t)}{2} \left[ \frac{1}{\sigma^2(M')} - \frac{1}{\sigma^2(M)} \right] \right\} dM'. \end{aligned} \quad (2)$$

In the SSM model, it is assumed that a halo with mass  $M$  experiences a merger and is destroyed when the relative mass increment  $\Delta M/M \equiv (M' - M)/M$  exceeds a certain threshold  $\Delta_m$ . The merger is regarded as the formation of a new halo. On the other hand, when  $\Delta M/M < \Delta_m$ , the event is regarded as continuous accretion; the halo keeps its identity

and its structure. Thus, from the specific merger rate (equation [2]), the mass accretion rate,  $R_{\text{mass}}(M, t) \equiv dM/dt$ , of halos with mass  $M$  at time  $t$  is defined as

$$R_{\text{mass}}(M, t) = \int_M^{M(1+\Delta_m)} \Delta M r_{\text{LC}}^m(M \rightarrow M', t) dM'. \quad (3)$$

The destruction rate of halos is defined as

$$r^d(M, t) = \int_{M(1+\Delta_m)}^{\infty} r_{\text{LC}}^m(M \rightarrow M', t) dM'. \quad (4)$$

On the other hand, the formation rate of halos is given by

$$r^f[M(t), t] = \frac{d \ln n[M(t), t]}{dt} + r^d[M(t), t] + \frac{\partial R_{\text{mass}}[M(t), t]}{\partial M}, \quad (5)$$

which follows from the conservation equation for the number density of halos per unit mass along mean mass accretion tracks,  $M(t)$ , which is obtained by solving the differential equation

$$\frac{dM}{dt} = R_{\text{mass}}[M(t), t]. \quad (6)$$

From the formation rate, we can obtain the distribution of formation times for halos with masses  $M_0$  at the present time  $t_0$ ;

$$\Phi_f(t; M_0, t_0) dt = r^f[M(t), t] \exp \left\{ - \int_t^{t_0} r_f[M(t'), t'] dt' \right\} dt, \quad (7)$$

where  $\Phi_f(t; M_0, t_0) dt$  gives the probability that a clusters with a mass  $M_0$  at the present time ( $t_0$ ) had its last major merger during the time period  $t \rightarrow t + dt$ . The median of this distribution is adopted as the typical halo formation time or the last merger time,  $t_f$ .

The value of  $\Delta_m$  is fixed by the fits to the empirical mass-density (or mass-radius) correlation obtained by  $N$ -body simulations (Navarro, Frenk, & White 1997). Salvador-Sole, Solanes, & Manrique (1998) showed that the best fit is  $\Delta_m = 0.6$  in a number of different cosmological models. In other words, the core structure of halos are destroyed when  $\Delta_m \gtrsim 0.6$ . We use this value in §3. Although merger and accretion cannot be distinguished clearly and the value has a range ( $0.5 \lesssim \Delta_m \lesssim 0.7$ ), the simple distinction would make the results of calculations easy to understand. On the other hand, hydrodynamical simulations of clusters show that smaller mergers can still produce internal shocks and violent hydrodynamical activity in clusters especially when they are binary mergers (e.g., the  $\Delta M/M = 1/8$  mergers in Roettiger, Burns, & Stone [1999] or the  $\Delta M/M = 1/3$  mergers in Ricker & Sarazin [2001]). These smaller mergers ( $0.1 \lesssim \Delta M/M \lesssim 0.6$ ) are often observed as “mergers”, although they do not significantly change the dark matter structure of main clusters *in the*

*end*; they only extend the density distribution (Salvador-Sole, Solanes, & Manrique 1998; Navarro, Frenk, & White 1997). Since ICM is in pressure equilibrium with the dark matter potential except during the mergers, we expect that those “semi-mergers” do not significantly change the ICM structure in the end, either. In §3, we will discuss the nonthermal emission from the semi-mergers, which are included in accretion in our classification unless otherwise mentioned.

## 2.2. Shock Acceleration of Electrons at the Cluster Edge

The virial radius of a cluster with virial mass  $M(t)$  is defined as

$$r_{\text{vir}}(t) = \left[ \frac{3 M(t)}{4\pi \Delta_c(t) \rho_{\text{crit}}(t)} \right]^{1/3}, \quad (8)$$

where  $\rho_{\text{crit}}(t)$  is the critical density of the universe and  $\Delta_c(t)$  is the ratio of the average density of the cluster to the critical density at time  $t$ . The former is given by

$$\rho_{\text{crit}}(t) = \frac{\rho_{\text{crit},0} \Omega_0 (1+z)^3}{\Omega(t)}, \quad (9)$$

where  $\rho_{\text{crit},0}$  and  $\Omega_0 = \rho_0/\rho_{\text{crit},0}$  are the critical density and cosmological density parameter at present, and  $\Omega(t)$  is the cosmological density parameter, and  $z$  is the redshift corresponding to time  $t$ . The latter is given by

$$\Delta_c(t) = 18 \pi^2 + 82x - 39x^2, \quad (10)$$

for a flat universe with non-zero cosmological constant (Bryan & Norman 1998). In equation (10), the parameter  $x$  is given by  $x = \Omega(t) - 1$ .

We assume that a cluster is spherically symmetric and that a shock is formed at the virial radius of a cluster (Evrard, Metzler, & Navarro 1996; Takizawa & Mineshige 1998; Eke, Navarro, & Frenk 1998). Since we adapt a rather large upper mass cutoff for accretion, and hydrodynamical simulations show that shocks from smaller mergers penetrate much deeper into the cluster interior than  $r_{\text{vir}}$  (e.g., the  $\Delta M/M = 1/8$  mergers in Roettiger, Burns, & Stone [1999] or the  $\Delta M/M = 1/3$  mergers in Ricker & Sarazin [2001]), this assumption overestimates the radius at which nonthermal effects due to accretion occur. However, as will be shown in §3.1, the contribution of such semi-mergers to the nonthermal emission due to accretion is not large in general. For continuous accretion, spherical models indicate that the structure of a cluster does not change much inside the shock radius (Takizawa & Mineshige 1998). Thus, we assume that the mass of a cluster between radii  $r = r_{\text{vir}}(t_i)$  and

$r_{\text{vir}}(t_i + \delta t_i)$  is  $M(t_i + \delta t_i) - M(t_i)$  for  $t_i > t_f$ . The virial mass of a cluster is obtained by solving equation (6) for a given virial mass at  $z = 0$ . The gravitational energy imparted to the baryon contained in the mass shell is approximately given by

$$E_b[r_{\text{vir}}(t_i), r_{\text{vir}}(t_i + \delta t_i)] \approx f_b \frac{1}{2} v_{\text{vir}}(t_i)^2 [M(t_i + \delta t_i) - M(t_i)], \quad (11)$$

where  $f_b$  is the baryon fraction. We use  $f_b = 0.25(h/0.5)^{-3/2}$ , where the present value of the Hubble constant is written as  $H_0 = 100 h \text{ km s}^{-1} \text{ Mpc}^{-1}$ . The value of  $f_b$  is the observed ICM mass fraction of high-temperature clusters (Mohr, Mathiesen, & Evrard 1999; Ettori & Fabian 1999; Arnaud & Evrard 1999), for which the effect of heating other than gravity is expected to be small (e.g., Cavaliere, Menci, & Tozzi 1998; Fujita & Takahara 2000; Loewenstein 2000). In equation (11),  $v_{\text{vir}}$  is the velocity of the mass shell just before it reaches  $r = r_{\text{vir}}(t_i)$ , which is given by

$$\frac{1}{2} v_{\text{vir}}(t_i)^2 = \frac{GM(t_i)}{r_{\text{vir}}(t_i)} - \frac{GM(t_i)}{r_{\text{ta}}[r_{\text{vir}}(t_i)]}. \quad (12)$$

In this equation,  $r_{\text{ta}}[r_{\text{vir}}(t_i)]$  is the turn around radius of the mass shell and is given by  $r_{\text{ta}}[r_{\text{vir}}(t_i)] = 2r_{\text{vir}}(t_i)$  on the basis of virial theorem.

We expect that some particles are accelerated to relativistic energies by the shock formed by accretion, and that the high-energy electrons radiate nonthermal emission. In this paper, we consider only the electrons directly accelerated at the shock (primary electrons), and ignore the electrons produced as secondaries by cosmic ray interactions (secondary electrons). This is because nonthermal protons, which are the source of the secondary electrons, accumulate in a cluster throughout its life (Blasi 2001); in order to calculate the evolution of the proton population, we may need to follow the entire merging history of the cluster.

We assume that an energy  $\xi_e E_b$  goes into the accelerating electrons. From observations of supernova remnants, we assume  $\xi_e = 0.05$  (Koyama et al. 1995; Tanimori et al. 1998). Let  $N(\gamma, t) d\gamma$  be the number of relativistic electrons with Lorentz factors in the range  $\gamma \rightarrow \gamma + d\gamma$  per unit volume, and let  $N_i(\gamma_i, t_i)$  be the initial electron density injected by acceleration at the accretion shock. We assume that the particles are accelerated with a power-law energy distribution,  $N_i(\gamma_i, t_i) = N_1 \gamma_i^{-p_0}$ . The normalization  $N_1$  is given by the relation

$$\int_{\gamma_{\text{min}}}^{\infty} m_e c^2 (\gamma_i - 1) N_i(\gamma_i, t_i) d\gamma_i = \xi_e \frac{E_b[r_{\text{vir}}(t_i), r_{\text{vir}}(t_i + \delta t_i)]}{(4\pi/3) [r_{\text{vir}}(t_i + \delta t_i)^3 - r_{\text{vir}}(t_i)^3]}, \quad (13)$$

where  $m_e$  is the electron mass and  $c$  is the light speed. Following Sarazin (1999), we use  $\gamma_{\text{min}} = 300$  and  $p_0 = 2.3$ . Note that the particle spectrum extends to  $\gamma < 300$ .

Electrons accelerated at  $r = r_{\text{vir}}(t_i)$  and  $t = t_i$  lose their energy through inverse Compton (IC) scattering of cosmic microwave background (CMB), synchrotron radiation, Coulomb



loss, and bremsstrahlung radiation. The energy loss rates are respectively given by

$$b_{\text{IC}}(\gamma) = 1.37 \times 10^{-20} \gamma^2 (1+z)^4 \text{ s}^{-1}, \quad (14)$$

$$b_{\text{syn}}(\gamma) = 1.30 \times 10^{-21} \gamma^2 \left( \frac{B}{1 \mu\text{G}} \right)^2 \text{ s}^{-1}, \quad (15)$$

$$b_{\text{Coul}}(\gamma) \approx 1.2 \times 10^{-12} n_e \left[ 1.0 + \frac{\ln(\gamma/n_e)}{75} \right] \text{ s}^{-1}, \quad (16)$$

$$b_{\text{brem}}(\gamma) \approx 1.51 \times 10^{-16} n_e \gamma [\ln(\gamma) + 0.36] \text{ s}^{-1}, \quad (17)$$

where  $B$  is the magnetic field and  $n_e$  is the thermal electron density (Blumenthal and Gould 1970; Rephaeli 1979; Sarazin 1999). The evolution of the energy of an electron is described by

$$\frac{d\gamma}{dt} = -b(\gamma, t), \quad (18)$$

where  $b = b_{\text{IC}} + b_{\text{syn}} + b_{\text{Coul}} + b_{\text{brem}}$ . We assume that the accelerated electrons remain in the same place. (In §3.1, we discuss the validity of this assumption.) Moreover, we assume that there is no additional injection of particles at a certain radius after a shock moves outwards. Thus, the differential population density in a mass shell for  $t > t_i$  is given by

$$N(\gamma, t) = N_i(\gamma_i, t_i) \left. \frac{\partial \gamma_i}{\partial \gamma} \right|_t. \quad (19)$$

The electron density in a mass shell between  $r_{\text{vir}}(t_i)$  and  $r_{\text{vir}}(t_i + \delta t_i)$  is assumed to be

$$n_e = \frac{3}{4\pi} \frac{0.86}{m_H} \frac{M(t_i + \delta t_i) - M(t_i)}{r_{\text{vir}}(t_i + \delta t_i)^3 - r_{\text{vir}}(t_i)^3}, \quad (20)$$

where  $m_H$  is the mass of hydrogen. Here, we assumed that the metal abundance of the ICM is 0.3 solar abundance. We assume that magnetic field in a cluster is adiabatically compressed. Thus, the magnetic field in the mass shell is given by

$$B = B_0 (n_e/n_{e0})^{2/3} \quad (21)$$

where  $n_{e0}$  is the electron density of the background universe and  $B_0$  is a parameter. We use  $B_0 = 0.01 \mu\text{G}$  unless otherwise mentioned; the value is consistent with observed synchrotron emission from clusters (§4). We assume that the magnetic field at a fixed location does not change after the passage of the accretion shock. Note that the cooling time of most of the accelerated electrons is relatively short except for lower energy electrons which make EUV emission (Sarazin 1999). Thus, a slow change of the internal structure of clusters does not strongly affect the present nonthermal emission from the electrons except for the EUV.

### 2.3. Mergers

In the SSM model, a cluster is assumed to experience a merger when  $\Delta M/M > \Delta_m$ . In violent mergers, shocks will propagate through the ICM of the merger remnant, and these shocks should accelerate particles throughout the whole cluster. In this case, the emission from the nonthermal particles comes not only from the outer region but also from the central region of the cluster (see Figs. 3 and 4 in Takizawa & Naito 2000). In this subsection, we construct a model to estimate the nonthermal emission of merging clusters using a spherical collapse model.

When a cluster is approximated by an isothermal sphere, the gravitational energy is given by

$$E_G \approx \frac{3}{4} \frac{GM^2}{r_{\text{vir}}}. \quad (22)$$

Thus, a similar amount of energy should be released at the merger that makes a cluster with the mass of  $M$  (Totani & Kitayama 2000). We consider only the last merger, which occurred at  $t = t_f$ . The cluster mass just after the merger is given by  $M(t_f)$ , where  $M(t)$  is the solution of equation (6) for a given present mass. The virial radius  $r_{\text{vir}}$  is given by equation (8). We assume that the energy  $E_{\text{e,mer}} = \xi_e f_b E_G$  goes to accelerated electrons by the merger.

We assume that the shock velocity in a merging cluster is  $V_s = (4/3)V_f$ , which is the velocity of a strong shock when a material is shocked by a supersonic piston with a velocity of  $V_f$ . Note that if the Mach number of the shock is  $\sim 2$ , the shock velocity increases by  $\sim 30\%$ . We define the velocity as  $V_f \approx \sqrt{GM/r_{\text{vir}}}$  e.g., the infall velocity of material from  $r = 2r_{\text{vir}}$ . The time for the shock wave to propagate across the radius of the cluster is  $t_{\text{shock}} = r_{\text{vir}}/V_s$ . Thus, during a merger, the energy injection rate to accelerated electrons is assumed to be  $E_{\text{e,mer}}/t_{\text{shock}}$ . The accelerated electrons lose their energy by the same processes as in the accretion model (equations [14]-[17]). As the electron density around the shock front in a merging cluster, we use a typical density;

$$n_e = f_b \frac{0.86M}{m_H(4\pi/3)r_{\text{vir}}^3}, \quad (23)$$

For the magnetic field around the shock front, we use equation (21). We use  $\xi_e = 0.05$  and  $B_0 = 0.01 \mu\text{G}$  as is the case of the accretion unless otherwise mentioned.

### 3. Results

We consider several models with differing cosmological parameters and values for the present mass of the cluster. Table 1 shows the density parameter  $\Omega_0$ , the cosmological constant  $\lambda$ , the Hubble constant parameter  $h$ , the present rms density fluctuation in  $8 h^{-1}$  Mpc spheres  $\sigma_8$ , the present mass of a cluster  $M_0 \equiv M(z = 0)$ , and the magnetic field  $B_0$ . The masses  $M_0 = 10^{15} M_\odot$  and  $M_0 = 10^{14} M_\odot$  correspond to clusters of galaxies and groups of galaxies, respectively. Figure 1 shows the probability distributions of the last merger of clusters. The arrows in the figure indicate the median of the distributions or the typical redshifts at which last mergers occurred,  $z_f = z(t_f)$ .

#### 3.1. The Emission from a Cluster Undergoing Accretion

We solve the equation (6) and derive the evolution of the virial mass of a cluster after the last merger (Figure 2). To emphasize accretion, the curves are computed assuming the last merger occurred at  $z > 2$ . The mass of a cluster in the Einstein-de Sitter universe (models S1 and S2) decreases more rapidly with redshift than in a low density universe (models L1 and L2), although the difference is not large.

Figures 3 and 4 respectively show the distributions of gas density and magnetic fields. The right ends of the curves correspond to the present virial radius of clusters. The arrows in the figures indicate  $r_{\text{vir}}(t_f)$ . Given the simplifying assumptions, the density profiles may not be very realistic. In particular, for  $r \lesssim r_{\text{vir}}(t_f)$ , mergers may affect the structure of the gas. However, since the cooling time of high energy electrons is smaller than the time scale for changes to the cluster structure, the inaccuracy of the density profile in the inner region of a cluster does not affect the nonthermal emission from the electrons. (EUV emission may be affected because electrons responsible for it have relatively large cooling time [Sarazin 1999].) Moreover, for  $r \gtrsim r_{\text{vir}}(t_f)$ , the density profiles are roughly  $n_e \propto r^{-2.3}$ , which is roughly consistent with the outer part of the so-called universal density profile (Navarro, Frenk, & White 1996, 1997). Since the universal density profile is often claimed to represent the actual density profiles of dark matter well, the obtained profiles in Figure 3 may not be unrealistic at least for their outer parts. Note that we implicitly assumed that the density profile of ICM follows that of dark matter or assumed that the effect of non-gravitational heating is small. This assumption is good at least for massive clusters (e.g., Cavaliere, Menci, & Tozzi 1998; Fujita & Takahara 2000; Loewenstein 2000); for smaller clusters some modification may be required but it is beyond our scope in this paper. Since the following results are not much different between model series L and S, we present the results of models L1 and L2 in the rest of this subsection.

Using the profiles of magnetic fields, we can estimate the diffusion length of electrons. The diffusion coefficient of relativistic electrons is given by

$$D_{\text{CR}}(E) \approx 5.0 \times 10^{29} \left( \frac{E}{1 \text{ GeV}} \right)^{1/3} \left( \frac{B}{0.1 \mu\text{G}} \right)^{-1/3} \text{ cm}^2 \text{ s}^{-1}, \quad (24)$$

where  $E$  is the energy of an electron (Berezinsky, Blasi, & Ptuskin 1997; Colafrancesco & Blasi 1998). The distance which an electron reaches before being affected by cooling is given by

$$l_D \approx \sqrt{6D_{\text{DR}}t_{\text{cool}}} \approx 100 \left( \frac{E}{1 \text{ GeV}} \right)^{1/6} \left( \frac{B}{0.1 \mu\text{G}} \right)^{-1/6} \left( \frac{t_{\text{cool}}}{1 \text{ Gyr}} \right)^{1/2} \text{ kpc}, \quad (25)$$

where  $t_{\text{cool}}$  is the cooling time of an electron. Assuming  $t_{\text{cool}} = 1/b(\gamma, t)$ , we calculate  $l_D$  and present it in Figure 5 for an electron at  $r \sim r_{\text{vir}}(z = 0)$  for models L1 and L2. Since  $l_D$  is much smaller than the virial radius of clusters, diffusion does not affect the radial profile of nonthermal emission from the high-energy electrons significantly. In particular, synchrotron and hard X-ray emissions are not affected by the diffusion because higher energy electrons ( $\gamma \gtrsim 10^4$ ) are responsible for them.

Figure 6 shows the spectra of the total emission of a cluster. The overall profiles are similar to those in steady injection models in Sarazin (1999). The absolute values of the power are smaller than those of models 1 and 20 in Sarazin (1999) because of smaller injection rate of high-energy electrons in our models.

In Figure 7, we present the radial dependence of the electron spectra. As the radius decreases, electron cooling affects the electron population because the electrons were accelerated at earlier times. In particular, IC scattering greatly reduces the number of higher energy electrons (see Sarazin 1999). As a result, the upper cutoff of electron spectra decreases (Figure 7). Figure 8 shows the radial dependence of the synchrotron and IC emissivity of the cluster as a function of frequency. In the inner region, the lack of high-energy electrons reduces the synchrotron and IC emission at higher frequencies. In particular, radio synchrotron emission should exist only at  $r \sim r_{\text{vir}}$ .

Figure 9 shows the surface brightness profiles of the nonthermal emission for several frequencies. Since most of the emission, especially in radio and hard X-ray ranges, comes from the outer region of clusters (Figure 8), the profiles are almost constant in the inner regions. Since synchrotron emission and IC emission at larger frequency are strictly limited to the cluster edge (Figure 8), their surface brightness distributions show humps near the right ends of the curves or at  $r \sim r_{\text{vir}}$  (Figure 9). Figure 8 suggests that the emission from the region of  $r \lesssim r_{\text{vir}}(t_f)$  ( $\sim 1.5$  Mpc for model L1 and  $\sim 0.5$  Mpc for model L2) does not contribute to the surface brightness profiles at the frequencies in Figure 9 except that at  $\nu = 10^{16}$  Hz in model L2.

As is mentioned in §2, “semi-mergers” ( $0.1 \lesssim \Delta_m \lesssim 0.6$ ) can produce internal shocks. Thus, it is likely that the nonthermal effects of “semi-mergers” penetrate further into the cluster interior than we calculated on the assumption of accretion. The effect of semi-mergers on the nonthermal emission due to the accretion in our sense can be estimated as follows. Assuming that the mass evolution of clusters is described by Figure 2 and assuming that the average density and magnetic field profiles are given by Figures 3 and 4, respectively, the contribution of “pure-accretion” ( $0 \lesssim \Delta_m \lesssim 0.1$ ) to the nonthermal emission due to the accretion is

$$f_{\text{pure}}(t) \approx \int_M^{1.1M} \Delta M r_{\text{LC}}^m(M \rightarrow M', t) dM' / \int_M^{1.6M} \Delta M r_{\text{LC}}^m(M \rightarrow M', t) dM', \quad (26)$$

where  $M = M(t)$  is shown in Figure 2. We found that  $f_{\text{pure}} = 0.4 - 0.6$  for essentially all of the models we studied at all times. That is, the emission due to the pure accretion is at most factor of two smaller than that shown Figure 6, 8, and 9. Thus, taking account of the simplicity of the model, even if we do not include semi-mergers in accretion, the results of this subsection do not change very significantly.

### 3.2. The Emission From a Merging or Merged Cluster

We assume that there are no nonthermal electrons in a cluster before the last merger for the sake of simplicity. Figure 10 shows the emission spectra from a merging or merged cluster observed at  $z = 0$  for models L1 and L2; the results of models S1 and S2 are similar to them. The emission from the particles accelerated via accretion is not included in the emission from the merging or merged cluster; it is shown separately in Figure 10.

For models L1 and L2, a cluster is still in a merging phase at  $z = 0$  if the merger starts at  $z \lesssim 0.1$ . During the merger, the radio emission and hard X-ray emission ( $\nu \gtrsim 10^{19}$  Hz) are almost constant. This is because the electrons responsible for these emissions have large energies ( $\gamma \gtrsim 10^4$ ), and thus short cooling times ( $\lesssim 10^8$  yrs; see Fig. 2 in Sarazin 1999). Since the energy injection rate for the nonthermal electrons is assumed to be constant (§2.3), the nonthermal emissions are also constant. However, the IC emission with  $\nu \lesssim 10^{17}$  Hz increases with the redshift at which the merger starts as long as the cluster is in the merger phase at  $z = 0$ , because the emission is attributed to the electrons with  $\gamma \lesssim 10^3$  and their cooling times are fairly long ( $\sim 10^9$  yrs); these electrons accumulate in the cluster without rapidly losing their energy.

For the IC emission, Figure 10 shows that the soft X-ray and EUV emission from a merging cluster is not much different from that from an accreting cluster with a similar

mass. For hard X-rays ( $\nu \gtrsim 10^{19}$  Hz), the ratio of the luminosity of a merging cluster to that of an accreting cluster simply reflects the ratio of their energy injection rates for nonthermal electrons, because the cooling time of the high-energy electrons responsible for the emissions is small in comparison with the time scales of merger and accretion. The ratio of their energy injection rates is approximately given by

$$\frac{L_{X,\text{mer}}}{L_{X,\text{acc}}} \sim \frac{GM^2/(r_{\text{vir}}^2 t_{\text{shock}})}{GM^2/(r_{\text{vir}}^2 t_0)} = \frac{t_0}{t_{\text{shock}}} \sim 10 \quad (27)$$

On the other hand, for  $\nu \lesssim 10^{17}$  Hz, the low-energy nonthermal electrons accumulated in an accreting cluster make the emission comparable to that from a merging cluster with similar mass.

In comparison with the IC emission, the difference in the synchrotron emission power between a merging cluster and an accreting cluster is larger (Figure 10). This is due to the combined effect of the large rate of energy injection to electrons and the large magnetic field in the interior of a merging cluster; the magnetic field in the merging cluster ( $\sim 0.1 \mu\text{G}$ ) exceeds that at the edge of the accreting cluster by a factor of three. If the ratio of the magnetic field strength averaged in a cluster to the magnetic field strength at the cluster edge is much larger than our model, as suggested by numerical simulations (Dolag & Enßlin 2000), an accreting cluster and a merging cluster would be even more disparate in radio power.

If a cluster merger starts at  $z \gtrsim 0.1$ , the merger has completed before  $z = 0$ . The present radio emission and hard X-ray emission ( $\nu \gtrsim 10^{18}$  Hz) due to the last merger rapidly decline with the redshift of the last merger because of the short cooling time of high-energy electrons. As soon as the merger finishes, these emissions become smaller than those due to ongoing accretion. On the contrary, the IC emission with  $\nu \lesssim 10^{17}$  Hz does not change much after the last merger because of the long cooling time of the relatively low-energy electrons; even for the cluster that experiences the last merger at  $z \sim 0.4$ , the EUV emission is still comparable to that from the edge of a cluster undergoing accretion.

In Table 2, we list the fraction ( $f_{\text{mer}}$ ) of clusters in a merging phase and the fraction ( $f_{\text{mer,EUV}}$ ) whose EUV luminosity ( $\nu \sim 10^{16-17}$  Hz) attributed to their last merger is larger than that attributed to matter accretion, both at  $z = 0$ . The average redshift of cluster formation or the last merger ( $z_f$ ) and the equal EUV redshift ( $z_{\text{EUV}}$ ) are also presented; here, we define  $z_{\text{EUV}}$  such that, if a cluster experiences its last merger at  $z < z_{\text{EUV}}$ , the EUV luminosity due to the last merger is larger than that due to the accretion at  $z = 0$ . Table 2 shows that only  $\sim 10\%$  of clusters at  $z \sim 0$  are in a merging phase and radiate strong radio emission due to the merger from their interior. The remaining clusters radiate weak radio emission due to accretion from the outskirts. The hard X-ray radiation of the  $\sim 10\%$  of

merging clusters is relatively strong and it comes from the interior of the cluster. The hard X-ray radiation of the accreting clusters is weaker about a factor of 10 and it is limited to their outer regions. Table 2 also suggests that 20 – 40% of clusters at  $z \sim 0$  should have EUV emission due to the last merger from the whole clusters and the rest should have that from the outer regions. However, for EUV emission, the distinction between merger and accretion may be difficult because the EUV emission from an accreting cluster is relatively uniform and extends to the inner region of the cluster (Figure 9).

The nonthermal emission from semi-mergers ( $0.1 \lesssim \Delta_m \lesssim 0.6$ ) may come from the inner regions of clusters (§2). The luminosity due to nonthermal emission from a cluster undergoing a semi-merger is expected to be  $\gtrsim 10\%$  of that from a cluster undergoing a merger ( $\Delta_m \gtrsim 0.6$ ), because the typical ICM density and magnetic fields are expected to be the same for both clusters and the luminosity is proportional to the kinetic energy of the merged subclusters. Figure 11 is the same as the Figure 10 but the merger luminosity is set to be 20% of that in Figure 10 and the accretion luminosity is set to be a half of that in Figure 10. That is, they respectively represent a typical “semi-merger” and “pure accretion”. As is seen, the luminosity due to a semi-merger is between that due to pure accretion (or accretion) and that due to a merger for hard X-ray and radio emissions (Figure 10 and 11). Table 2 also shows the fraction of clusters undergoing semi-mergers or mergers ( $f_{\text{smr}}$ ), which is calculated from the probability distribution,  $\Phi_f(z)$  for  $\Delta_m = 0.1$ . As can be seen,  $f_{\text{smr}} \sim 0.2 - 0.3$  for a low density universe (models L1 and L2) and  $f_{\text{smr}} \sim 0.3 - 0.4$  for the Einstein de-Sitter universe (models S1 and S2). Considering the short cooling time of high energy electrons, these fractions of clusters should have hard X-ray and radio emissions due to the semi-mergers or mergers.

### 3.3. Magnetic Fields

The magnetic fields derived from observed hard X-ray and EUV emissions on the assumption that these are IC scattering of CMB photons are rather low ( $\sim 0.2 \mu\text{G}$ ; Fusco-Femiano et al. 1999, 2000). On the other hand, analysis of rotation measure suggests that the magnetic fields in clusters should be larger a factor of 10 – 100 (e.g., Lawler & Dennison 1982; Kim et al. 1990; Goldshmidt & Rephaeli 1993; Clarke, Kronberg, & Böhringer 2001). Our default parameter ( $B_0 = 0.01 \mu\text{G}$ ) gives the magnetic fields compatible with the former. In this subsection, we investigate the magnetic fields compatible with the latter.

We ran a model with  $B_0 = 0.1 \mu\text{G}$ ; the other parameters are the same as in model L1. We refer to this model as model L1'. In this model, the magnetic field is 10 times as large as that in model L1. Thus, for an accreting cluster, the magnetic field in the central region

is  $\sim 10 \mu\text{G}$  and that at the cluster edge is  $0.5 \mu\text{G}$ . The magnetic field of a merging cluster is  $1.3 \mu\text{G}$ . Figure 12a shows the total emission from the cluster. The IC emission in model L1' is not much different from that in model L1 because the IC emission is not much affected by the change of magnetic fields as long as  $B \lesssim 1 \mu\text{G}$  (Sarazin 1999). On the contrary, the synchrotron luminosity in model L1' is much larger than that in model L1, because the synchrotron emission is proportional to  $B^2$  for a given population of high-energy electrons.

## 4. Discussion

In this section, we compare the results in §3 with observations. We use the cosmological parameters for model L (Table 1) or  $\Omega_0 = 0.7$ ,  $\lambda = 0.3$  and  $h = 0.7$ . Unfortunately, excess EUV and hard X-ray fluxes have been detected from only a few clusters so far, and thus we cannot discuss the emission statistically. Instead, we check the crude consistency between our simple model and observations for the individual clusters. On the other hand, thanks to the better sensitivity of radio telescopes, the number of clusters in which diffuse radio emission is detected is increasing, although the numbers may still be a bit small for detailed statistical analysis.

### 4.1. EUV/Soft X-ray Emission

Extreme ultraviolet (EUV) or very soft X-ray excess emission have been detected from a number of clusters (Lieu et al. 1996a,b; Bowyer, Lampton, & Lieu 1996; Bowyer & Berghöfer 1998; Mittaz, Lieu, & Lockman 1998; Kaastra et al. 1999; Lieu, Bonamente, & Mittaz 1999; Lieu et al. 1999; Berghöfer, Bowyer, & Korpela 2000a; Bonamente, Lieu, & Mittaz 2001). although it should be noted that the EUV detections remain controversial (Arabadjis & Bregman 1999; Bowyer, Berghöfer, & Korpela 1999; Berghöfer, Bowyer, & Korpela 2000b). Bonamente, Lieu, & Mittaz (2001) detected excess EUV emission from A1795 and found that the total EUV luminosity is  $\sim 3 \times 10^{43} \text{ ergs s}^{-1}$  for 60 – 250 eV. The luminosity is consistent with model L1 series for both accretion and merger (Figure 10a, 11a and 12). However, the observed emission is restricted to the region of  $r \lesssim 700 \text{ kpc}$  for the cosmological parameters we used, which is inconsistent with the spread of the emission that our accretion model predicts (Figure 9a). As for A2199, Coma, and Virgo cluster, the same can be said (Lieu et al. 1999; Bowyer & Berghöfer 1998; Berghöfer, Bowyer, & Korpela 2000b). For an example, Kaastra et al. (1999) found excess emission from cluster A2199 in the 0.1 – 0.3 keV band. Although the luminosity,  $\sim 6 \times 10^{42} \text{ ergs}^{-1}$ , is consistent with model L1 series (Figure 10a, 11a, and 12), the emission is mainly limited to the region of  $\lesssim 400 \text{ kpc}$  and is inconsistent



with our prediction in the case of accretion (Figure 9a). These results suggest that the observed EUV emission is at least not attributable to the outer accretion shocks at the virial radius in clusters. On the other hand, the surface brightness of the EUV/soft X-ray emission produced by accretion is quite low, and is probably below the detection limit of the existing observations. Thus, the observations probably do not rule out accretion generated emission at the level predicted by the models, and even the reports of non-detection of EUV in clusters (Arabadjis & Bregman 1999; Bowyer, Berghöfer, & Korpela 1999; Berghöfer, Bowyer, & Korpela 2000b) may not be inconsistent with the accretion models.

## 4.2. Hard X-ray Emission

Excess hard X-ray emission has been detected in two clusters, Coma and Abell 2256. There is weaker evidence for hard X-ray excesses in Abell 2199 (Kaastra et al. 1999) and Abell 3667 (Fusco-Femiano et al. 2001). In Coma, the detection was made with both *BeppoSAX* (Fusco-Femiano et al. 1999) and *RXTE* (Rephaeli, Gruber, & Blanco 1999). For Coma cluster, the *BeppoSAX* hard X-ray flux is  $2.2 \times 10^{-11}$  ergs cm $^{-2}$  s $^{-1}$  in the 20 – 80 keV band. This corresponds to the luminosity of  $\sim 10^{43}$  ergs s $^{-1}$ , which is consistent with the prediction of model L1 for accretion (Figure 10a, 11a and 12). However, it is smaller than the model for a major merger ( $\sim 10^{44}$  ergs s $^{-1}$ ), although Coma Cluster is known as a merging cluster (e.g., Briel, Henry, & Böhringer 1992; Vikhlinin, Forman, & Jones 1997; Honda et al. 1996; Watanabe et al. 1999). The small luminosity suggests that the ratio of mass between the main cluster and the merger subcluster or subclusters fairly be large. For Abell 2256, which is also known as a merging cluster (e.g., Briel et al. 1991; Miyaji et al. 1993; Briel & Henry 1994; Markevitch 1996; Molendi, De Grandi, & Fusco-Femiano 2000), the flux of hard X-ray emission is  $1.2 \times 10^{-11}$  ergs cm $^{-2}$  s $^{-1}$  in the 20 – 80 keV band range (Fusco-Femiano et al. 2000). The corresponding luminosity is  $\sim 10^{44}$  ergs s $^{-1}$ , which is consistent with the prediction of model L1 series for a merger (Figure 10a, 11a and 12). The observed radio luminosities for Coma and A2256 are  $1 \times 10^{40}$  and  $2 \times 10^{40}$  erg s $^{-1}$  at 1.4 GHz, respectively (Feretti 2000). Both these clusters have both a radio halo and a relic. By comparing the luminosities with the model L1 series, it can be shown that  $B_0$  must be  $0.01 \mu\text{G}$  or the average magnetic fields in the clusters much be  $\bar{B} \sim 0.1 \mu\text{G}$  whether the emission is due to a merger or to accretion (Figure 10a, 11a and 12). Future observations of the spatial distributions of the hard X-ray emission would be quite useful to investigate whether mergers or accretion are responsible for the hard X-ray emission, and whether the hard X-ray emission is spatially coincident with the radio halos and/or the relics.

Fukazawa et al. (2001) detected an excess of hard X-ray at energies above 4 keV from the group of galaxies HCG 62. In the 2 – 10 keV range, the observed hard X-ray flux is  $(1.0 \pm 0.3) \times 10^{-12}$  ergs cm $^{-2}$  s $^{-1}$ . This implies a luminosity of  $\sim 4 \times 10^{41}$  ergs s $^{-1}$ , which is consistent with the accretion of model L2 (Figure 10b and 11b). However, the emission is confined to the region of  $r \lesssim 200$  kpc, which is inconsistent with the result in Figure 9b (model L2). Thus, we can say at least that the observed hard X-ray emission is not produced by electron acceleration through matter accretion to the group. Note that there is no strong evidence of merger for this group (Fukazawa et al. 2001). There is no radio detection of a diffuse source in this group.

### 4.3. Radio Emission

In some clusters, radio relics and halos are observed. Considering their locations, the relics may be the synchrotron emission from accelerated electrons at the cluster edge. On the other hand, the radio halos may be produced by mergers. Enßlin et al. (1998) compiled the observational results of relics and showed that the luminosities are  $\sim 10^{40-42}$  ergs s $^{-1}$  assuming a simple power law between 10 MHz and 10 GHz. Recently, Giovannini, Tordi, & Feretti (1999) searched for new halo and relic candidates in the NRAO VLA Sky Survey and found 29 candidates; the luminosities of the candidates are  $\sim 10^{39-41}$  ergs s $^{-1}$  at  $\nu = 1.4$  GHz. Moreover, Kempner & Sarazin (2001) also searched for halos and relics in all of the Abell clusters that are visible in the Westerbork Northern Sky Survey and found 18 candidates; the luminosities of the candidates are  $\sim 10^{39.5-40.5}$  ergs s $^{-1}$  at  $\nu = 327$  MHz. Furthermore, Giovannini & Feretti (2000) also find diffuse radio emissions from 7 clusters with VLA and the luminosities are  $\sim 10^{39.5-40.5}$  ergs s $^{-1}$  at  $\nu = 0.3$  and 1.4 GHz. These are consistent with model L1 (Figure 10a and Figure 11a); the dispersion of luminosities can be explained by the difference between merger and accretion. On the other hand, the observed luminosities are not consistent with model L1' (Figure 12) as the clusters in which hard X-ray emission is detected. These may suggest that magnetic fields in clusters are generally small ( $B_0 \sim 0.01 \mu\text{G}$  or  $\bar{B} \sim 0.1 \mu\text{G}$ ).

We note that such weak magnetic fields are not consistent with the large values implied by Faraday rotation measurements (e.g., Lawler & Dennison 1982; Kim et al. 1990; Goldshmidt & Rephaeli 1993; Clarke, Kronberg, & Böhringer 2001). Our results suggest that this discrepancy exists generally for clusters. Several authors have suggested ways to reconcile this difference, such as spatial inhomogeneity of the magnetic field and/or the relativistic particles (Goldshmidt & Rephaeli 1993), nonthermal bremsstrahlung emission by semi-relativistic particles as the source of the hard X-ray emission in clusters rather than

IC (Enßlin, Lieu, & Biermann 1999; Sarazin & Kempner 2000), an anisotropic pitch angle distribution of electrons (Petrosian 2001), and a high-energy cutoff in the electron energy distribution (Brunetti et al. 2001; Petrosian 2001). It is beyond the scope of this paper to consider all of these possibilities in concert with the accretion and merger models we give. However, as an example we consider electron energy distributions with a high-energy cutoff. We construct a simple model with the same parameters as model L1', but with  $N_i = 0$  for  $\gamma_i > 10^4$ ; such an electron distribution may be achieved when electrons accelerated in the past are reaccelerated by mergers at present (Brunetti et al. 2001). The result is shown in Figure 13. Compared to Figure 12, radio luminosity is much smaller, while the IC emission is not much different for  $\nu < 10^{19}$  Hz. Thus, a higher magnetic field could be accommodated by this model.

Most of the observed relics are not spherically symmetric. Thus, some of them may not have originated from pure accretion but from mergers or semi-mergers. The latter is consistent with the fact that radio relics are not observed in all clusters but only those with other evidence for mergers, although the incompleteness of the existing samples is a concern. The lack of symmetry might indicate that both an accretion shock and a preexisting relativistic population (a “radio ghost”) may be required to produce a relic (Enßlin & Gopal-Krishna 2001). On the other hand, given the limited sensitivity and incompleteness of radio searches for relics, it is possible that most clusters have low surface brightness, nearly spherically symmetric relics due to accretion shocks. Also, nonthermal emission from accretion shocks may not be generally spherically symmetric. This might occur because the accretion is always associated with clustered matter, and thus occurs through the intermittent accretion of small blobs ( $\Delta_m \lesssim 0.1$ ). Given the short cooling time of high-energy electrons, this would lead to asymmetric radio emission (Figures 7 and 8). Alternatively, accretion may be asymmetric if it occurs largely from filamentary large scale structures (Enßlin et al. 1998). In this case, the sense of the asymmetries would tend to remain constant over time, and would align with the large scale structure. If the radio emission due to accretion is asymmetric, one would expect a similar asymmetric structure in the hard X-ray IC emission as well, because this emission originates from the same higher energy electrons as the synchrotron emission.

## 5. Conclusions

According to the theories of structure formation in the universe, most clusters at  $z \sim 0$  are not in a merging phase but are undergoing accretion. Thus, we have investigated the nonthermal emission from the electrons accelerated by shocks around the cluster edge formed through matter accretion to the cluster. We compared the emission with the nonthermal

emission from merging clusters. Moreover, we have shown the radial profiles of the non-thermal emission for accreting clusters. In order to estimate the accretion rate and the probability distribution of cluster merger, we used a modification of an extend Press & Schechter model. We assumed that the rate of energy injection to high-energy electrons is proportional to the released gravitational energy of accreted matter or subclusters. We considered the energy loss through inverse Compton (IC) scattering of cosmic microwave background (CMB), synchrotron radiation, Coulomb losses, and bremsstrahlung radiation.

The results of our calculations show that the nonthermal emission owing to the accretion is restricted to the outer region of clusters. In particular, the synchrotron emission and the IC emission at high frequency ( $\nu \gtrsim 10^{19}$  Hz) are limited to the periphery of clusters. Thus, the surface brightness profiles of the nonthermal emissions are almost flat in the inner region of clusters regardless of frequency. On the other hand, the surface brightness of the synchrotron emission and the IC emission at high frequency ( $\nu \gtrsim 10^{19}$  Hz) is enhanced at the cluster edge. The total IC emission from an accreting cluster is not much different from that from a merging cluster; for EUV emission, they are comparable, and for hard X-ray emission, the former is smaller than the latter a factor of 10. On the other hand, the synchrotron emission from an accreting cluster is about 100 times smaller than that from a merging cluster. We predict that about 10% of clusters at  $z \sim 0$  have hard X-ray and radio nonthermal emissions due to their last merger, which are comparable to or dominate those due to ongoing accretion. On the other hand, if we define a merger as an increase in the mass of the larger subcluster by at least 10% of its initial mass, about 20 – 30% (30 – 40%) of clusters at  $z \sim 0$  should have hard X-ray and radio nonthermal emissions due to the merger even in a low density universe (in the Einstein de-Sitter universe). We also predict that 20 – 40% of clusters have significant extreme ultraviolet (EUV) emission due to their last major merger.

We compare the results with observations of clusters. We find that both our accretion and merger models are energetically consistent with the EUV emission of clusters. However, the observed emission is concentrated to the cluster centers in contrast with our prediction of accretion. The total luminosity of hard X-ray emission via IC scattering appears to be consistent with the observations of clusters. By comparing the observed hard X-ray emission and radio synchrotron emission for individual clusters, it is shown that the average magnetic fields should be  $\sim 0.1 \mu\text{G}$  for our simple model. Recently, the number of clusters in which diffuse radio emission is detected is increasing. If the emission is synchrotron emission due to accretion or mergers, the magnetic energy of clusters may generally be as small as in the clusters in which hard X-ray emission has been detected. However, we also find that models with a high-energy cutoff in the electron energy distribution will accommodate larger magnetic fields, which are in better agreement with Faraday rotation measurements.

We thank T. Furusyo, N. Y. Yamasaki, T. Ohashi, M. Yamada, and M. Enoki for useful comments. C. L. S. was supported in part by the National Aeronautics and Space Administration through *XMM* grant NAG5-10075 and *Chandra* Award Numbers through *Chandra* Award Number GO0-1158X, GO0-1173X, GO1-2122X, and GO1-2123X. all issued by the *Chandra* X-ray Observatory Center, which is operated by the Smithsonian Astrophysical Observatory for and on behalf of NASA under contract NAS8-39073.

## REFERENCES

- Arabadjis, J. S., & Bregman, J. N. 1999, *ApJ*, 514, 607
- Arnaud, M., & Evrard, A. E. 1999, *MNRAS*, 305, 631
- Atoyan, A. M., & Völk, H. J. 2000, *ApJ*, 535, 45
- Berezinsky, V. S., Blasi, P., & Ptuskin, V. S. 1997, *ApJ*, 487, 529
- Berghöfer, T. W., Bowyer, S., & Korpela, E. 2000a, *ApJ*, 535, 615
- Berghöfer, T. W., Bowyer, S., & Korpela, E. 2000b, *ApJ*, 545, 695
- Bertschinger, E. 1985, *ApJS*, 58, 39
- Blasi, P. 2001, *Astroparticle Physics*, 15, 223
- Blumenthal, G. R., & Gould, R. J. 1970, *Rev. Mod. Phys.*, 42, 237
- Bonamente, M., Lieu, R., & Mittaz, J. P. D. 2001, *ApJ*, 547, L7
- Bowyer, S., & Berghöfer, T. W. 1998, *ApJ*, 506, 502
- Bowyer, S., Berghöfer, T. W., & Korpela, E. J. 1999, *ApJ*, 526, 592
- Bowyer, S., Lampton, M., & Lieu, R. 1996, *Science*, 274, 1338
- Briel, U. G., et al., 1991, *A&A*, 246, L10
- Briel, U. G., & Henry, J. P. 1994, *Nature*, 372, 439
- Briel, U. G., Henry, J. P., & Böhringer, H. 1992, *A&A*, 259, L31
- Brunetti, G., Setti, G., Feretti, L., & Giovannini, G. 2001, *MNRAS*, 320, 365
- Bryan, G. L., & Norman, M. L. 1998, *ApJ*, 495, 80

- Buote, D. A. 2001, *ApJ*, 553, L15
- Cavaliere, A., Menci, N., & Tozzi, P. 1998, *ApJ*, 501, 493
- Clarke, T. E., Kronberg, P. P., & Böhringer, H. 2001, *ApJ*, 547, L111
- Colafrancesco, S., & Blasi, P. 1998, *Astroparticle Physics*, 9, 227
- Dolag, K., & Enßlin, T. A. 2000, *A&A*, 362, 151
- Eke, V. R., Navarro, J. F., & Frenk, C. S. 1998, *ApJ*, 503, 569
- Enoki, M., Takahara, F., & Fujita, Y. 2001, *ApJ*, in press
- Enßlin, T. A., & Biermann, P. L. 1998, *A&A*, 330, 90
- Enßlin, T. A., Biermann, P. L., Klein, U., & Kohle, S. 1998, *A&A*, 332, 395
- Enßlin, T. A., & Gopal-Krishna 2001, *A&A*, 366, 26
- Enßlin, T. A., Lieu, R., & Biermann, P. L. 1999, *A&A*, 344, 409
- Ettori, S., & Fabian, A. C. 1999, *MNRAS*, 305, 834
- Evrard, A. E., Metzler, C. A., & Navarro, J. F. 1996, *ApJ*, 469, 494
- Feretti, L. 2000, preprint (astro-ph/0006379)
- Fujita, Y., & Takahara, F. 2000, *ApJ*, 536, 523
- Fukazawa, Y., Nakazawa, K., Isobe, N., Makishima, K., Matsushita, K., Ohashi, T., & Kamae, T. 2001, *ApJ*, 546, L87
- Fusco-Femiano, R., Dal Fiume, D., Feretti, L., Giovannini, G., Grandi, P., Matt, G., Molendi, S., & Santangelo, A. 1999, *ApJ*, 513, L21
- Fusco-Femiano, R., et al., 2000, *ApJ*, 534, L7
- Fusco-Femiano, R., Dal Fiume, D., Orlandini, M., Brunetti, G., Feretti, L., & Giovannini, G. 2001, *ApJ*, 552, L97
- Giovannini, G., Feretti, L., Venturi, T., Kim, K.-T., & Kronberg, P. P. 1993, *ApJ*, 406, 399
- Giovannini, G., Tordi, M., & Feretti, L. 1999, *New Astronomy*, 4, 141
- Giovannini, G., & Feretti, L. 2000, *New Astronomy*, 5, 335

- Goldshmidt, O., & Rephaeli, Y. 1993, *ApJ*, 411, 518
- Honda, H., et al., 1996, *ApJ*, 473, L71
- Hwang, C.-Y. 1997, *Science*, 278, 1917
- Jaffe, W. J. 1977, *ApJ*, 212, 1
- Kaastra, J. S., Lieu, R., Mittaz, J. P. D., Bleeker, J. A. M., Mewe, R., Colafrancesco, S., & Lockman, F. J. 1999, *ApJ*, 519, L119
- Kang, H., Rachen, J. P., & Biermann, P. L. 1997, *MNRAS*, 286, 257
- Kempner, J. C., & Sarazin, C. L. 2001, *ApJ*, 548, 639
- Kauffmann, G., & White, S. D. M. 1993, *MNRAS*, 261, 921
- Kim, K.-T., Kronberg, P. P., Dewdney, P. E., & Landecker, T. L. 1990, *ApJ*, 355, 29
- Kitayama, T., 1997, PhD thesis, Univ. Tokyo
- Koyama, K., Petre, R., Gotthelf, E. V., Hwang, U., Matura, M., Ozaki, M., & Holt, S. S. 1995, *Nature*, 378, 255
- Lacey, C., & Cole, S. 1993, *MNRAS*, 262, 627
- Lawler, J. M., & Dennison, B. 1982, *ApJ*, 252, 81
- Lieu, R., Mittaz, J. P. D., Bowyer, S., Breen, J. O., Lockman, F. J., Murphy, E. M., & Hwang, C.-Y. 1996, *Science*, 274, 1335
- Lieu, R., Mittaz, J. P. D., Bowyer, S., Lockman, F. J., Hwang, C.-Y., & Schmitt, J. H. M. 1996, *ApJ*, 458, L5
- Lieu, R., Bonamente, M., & Mittaz, J. P. D. 1999, *ApJ*, 517, L91
- Lieu, R., Bonamente, M., Mittaz, J. P. D., Durret, F., Dos Santos, S., & Kaastra, J. S. 1999, *ApJ*, 527, L77
- Loewenstein, M. 2000, *ApJ*, 532, 17
- Markevitch, M. 1996, *ApJ*, 465, L1
- Miniati, F., Ryu, D., Kang, H., Jones, T. W., Cen, R., & Ostriker, J. P. 2000, *ApJ*, 542,608
- Mittaz, J. P. D., Lieu, R., & Lockman, F. J. 1998, *ApJ*, 498, L17

- Miyaji, T., et al., 1993, *ApJ*, 419, 66
- Mohr, J. J., Mathiesen, B., & Evrard, A. E. 1999, *ApJ*, 517, 627
- Molendi, S., De Grandi, S., & Fusco-Femiano, R. 2000, *ApJ*, 534, L43
- Nakamura, T. T., & Suto, Y. 1997, *Prog. Theor. Phys.*, 97, 49
- Navarro, J. F., Frenk, C. S., & White, S. D. M. 1996, *ApJ*, 462, 563
- Navarro, J. F., Frenk, C. S., & White, S. D. M. 1997, *ApJ*, 490, 493
- Petrosian, V. 2001, *ApJ*, in press (astro-ph/0101145).
- Press, W. H., & Schechter, P. 1974, *ApJ*, 187, 425
- Rephaeli, Y. 1979, *ApJ*, 227, 364
- Rephaeli, Y., Gruber, D., & Blanco, P. 1999, *ApJ*, 511, L21
- Ricker, P. M., & Sarazin, C. L. 2001, *ApJ*, in press (astro-ph/0107210)
- Roettiger, K., Burns, J. O., & Stone, J. M. 1999, *ApJ*, 518, 603
- Roland, J. 1981, *A&A*, 93, 407
- Salvador-Sole, E., Solanes, J. M., & Manrique, A. 1998, *ApJ*, 499, 542
- Sarazin, C. L. 1999, *ApJ*, 520, 529
- Sarazin, C. L. & Kempner, J. C. 2000, *ApJ*, 533, 73
- Sarazin, C. L., & Lieu, R. 1998, *ApJ*, 494, L177
- Schlickeiser, R., Sievers, A., & Thiemann, H. 1987, *A&A*, 182, 21
- Takizawa, M., & Mineshige, S. 1998, *ApJ*, 499, 82
- Takizawa, M., & Naito, T. 2000, *ApJ*, 535, 586
- Tanimori, T., et al., 1998, *ApJ*, 497, L25
- Totani, T., & Kitayama, T. 2000, *ApJ*, 545, 572
- Vikhlinin, A., Forman, W., & Jones, C. 1997, *ApJ*, 474, L7



Watanabe, M., Yamashita, K., Furuzawa, A., Kunieda, H., Tawara, Y., & Honda, H. 1999, ApJ, 527, 80

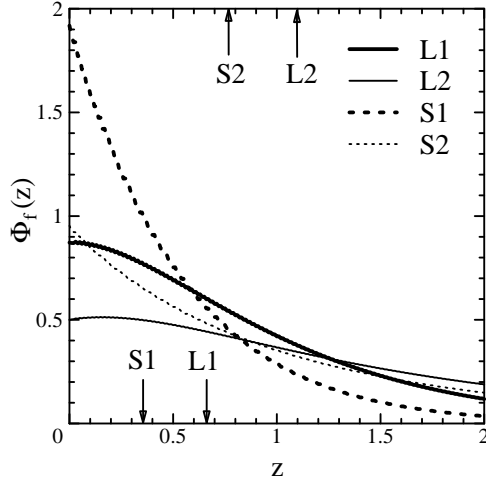


Fig. 1.— Probability distribution function  $\Phi_f(z)$  for the redshift  $z$  of the last merger for models L1 (thick solid line), L2 (thin solid line), S1 (thick dotted line), and S2 (thin dotted line).  $\Phi_f(z)$  is defined such that  $\Phi_f(z) dz$  gives the probability that the last major merger occurred between redshifts  $z$  and  $z+dz$ . The arrows indicate the median last merger redshift  $z_f = z(t_f)$ .

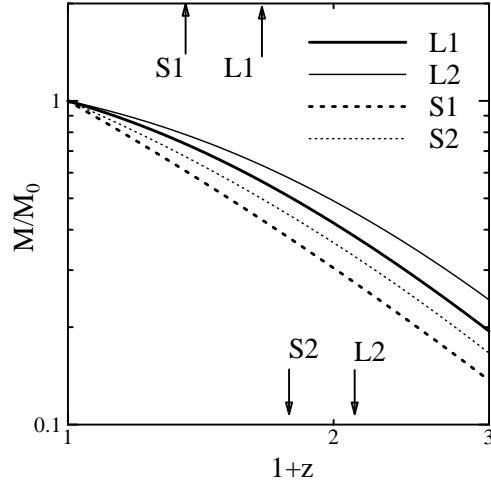


Fig. 2.— Evolution of the virial mass of a cluster for models L1 (thick solid line), L2 (thin solid line), S1 (thick dotted line), and S2 (thin dotted line), assuming only accretion occurs (eq. 6). The mass is normalized by the present-day mass  $M_0$ . The arrows indicate the median last merger redshift  $z_f = z(t_f)$ .

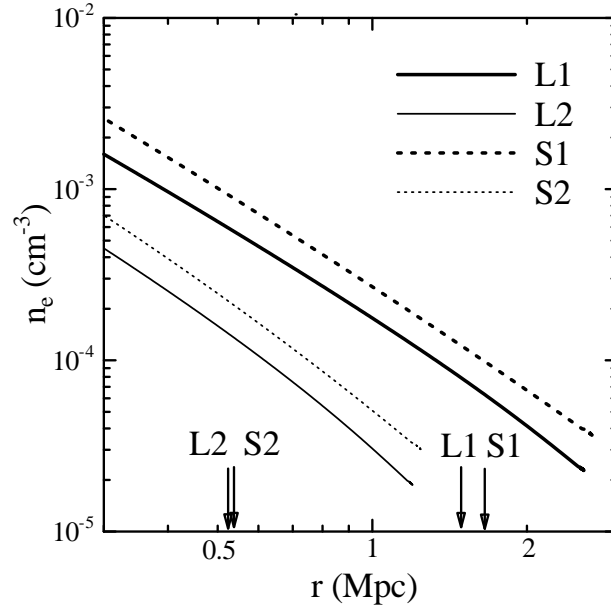


Fig. 3.— Gas density profiles for models L1 (thick solid line), L2 (thin solid line), S1 (thick dotted line), and S2 (thin dotted line). The arrows indicate the virial radius at the last merger  $r_{\text{vir}}(t_f)$ .

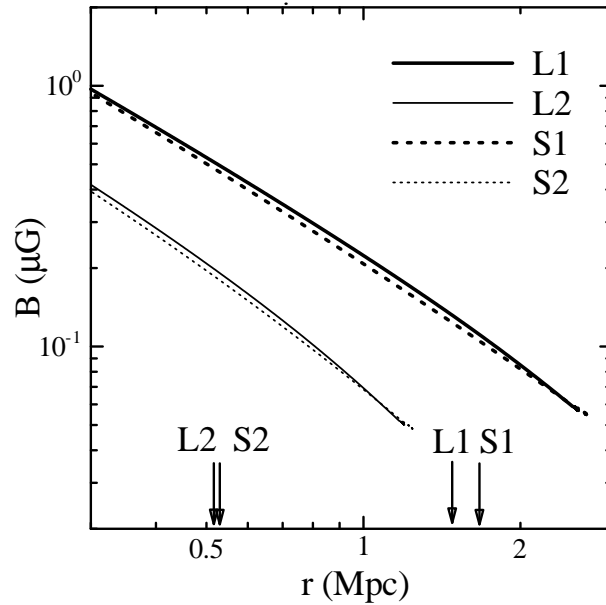


Fig. 4.— The same as Figure 3 but for magnetic field profiles.

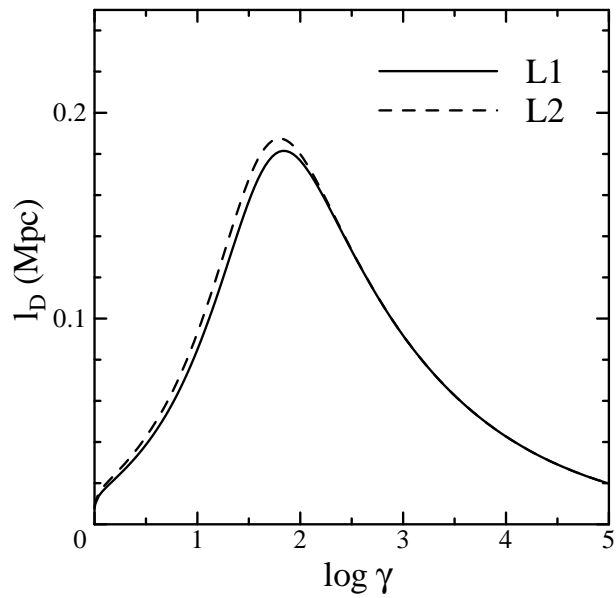


Fig. 5.— Diffusion length of an electron at the virial radius at  $z = 0$  for models L1 (solid line) and L2 (dashed line).

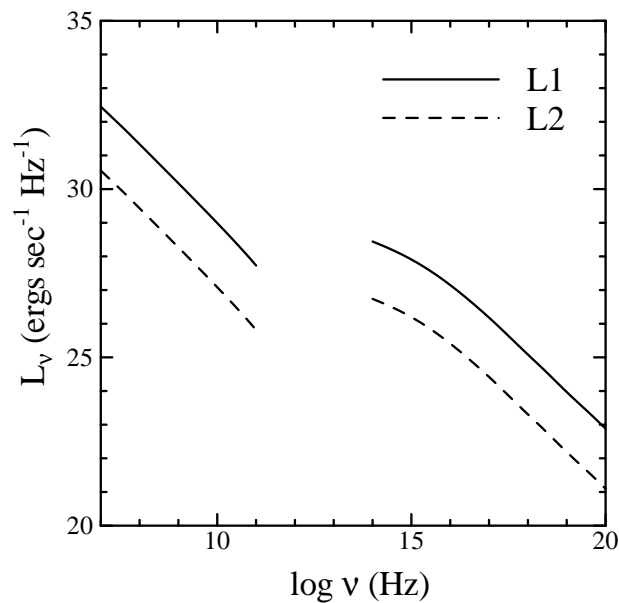


Fig. 6.— Spectra of total emission of a cluster for models L1 (solid line) and L2 (dashed line). The emission at  $\nu < 10^{11}$  Hz is synchrotron emission and the emission at  $\nu > 10^{14}$  Hz is IC emission.

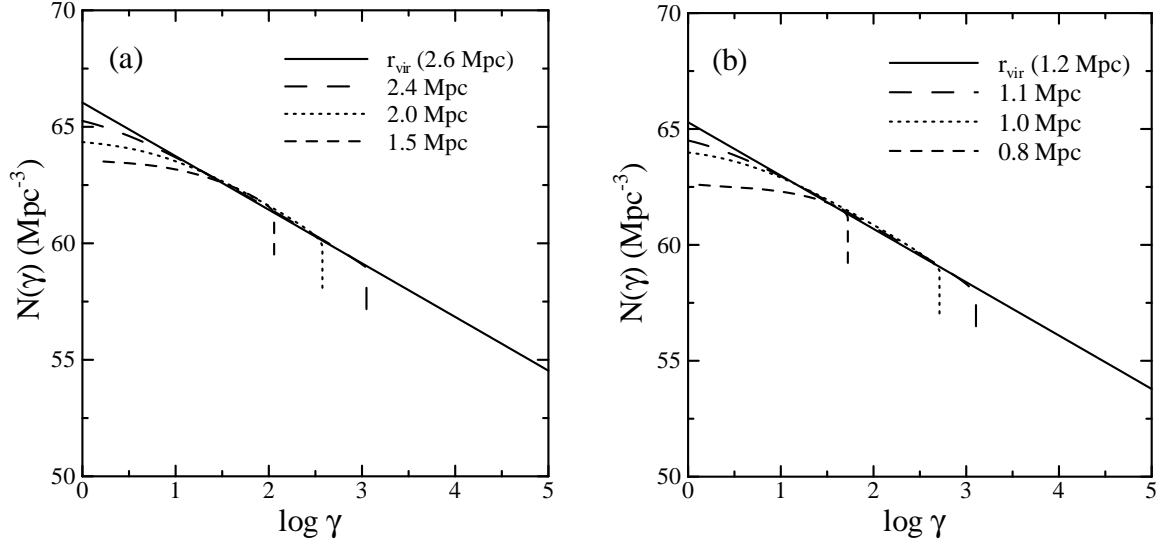


Fig. 7.— Radial dependence of electron spectra. (a) Model L1 (b) Model L2.

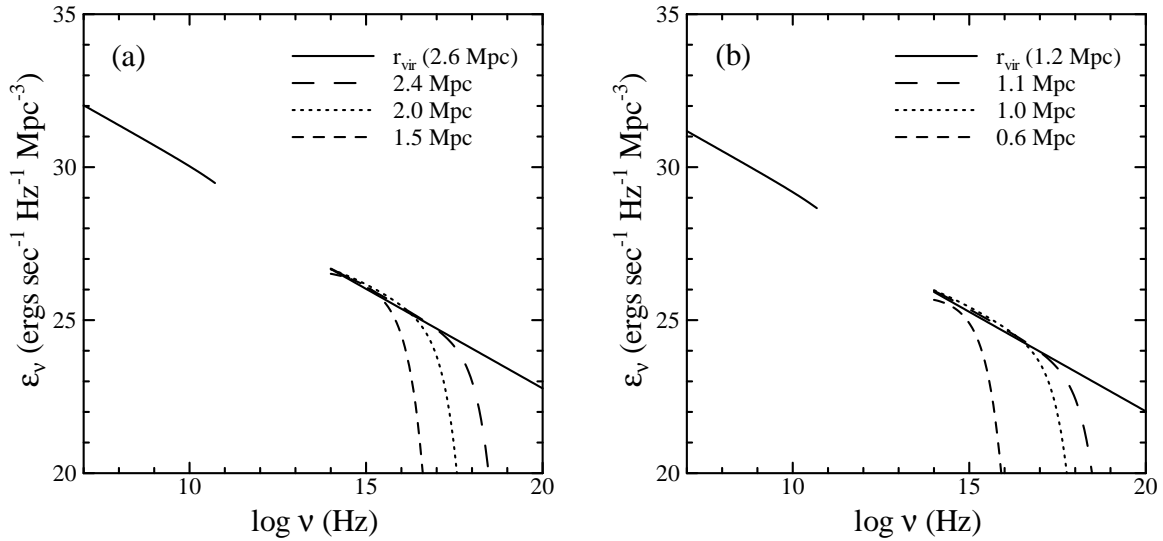


Fig. 8.— The radial distributions of the emissivity as a function of frequency for (a) model L1 and (b) model L2. The emission at  $\nu < 10^{11}$  Hz is synchrotron emission and that at  $\nu > 10^{14}$  Hz is IC emission. The radio emissivity at all radii below  $r_{\text{vir}}$  is too small to be plotted.

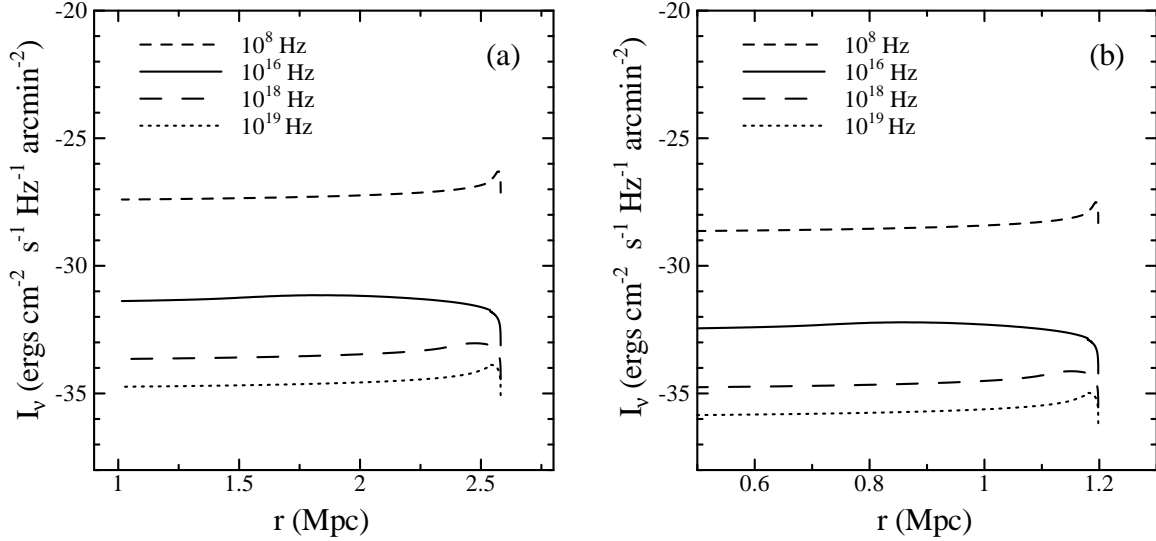


Fig. 9.— Surface brightness profiles of nonthermal emissions for several frequencies. The emission at  $\nu < 10^{11}$  Hz is synchrotron emission and that at  $\nu > 10^{14}$  Hz is IC emission. (a) Model L1 (b) Model L2.

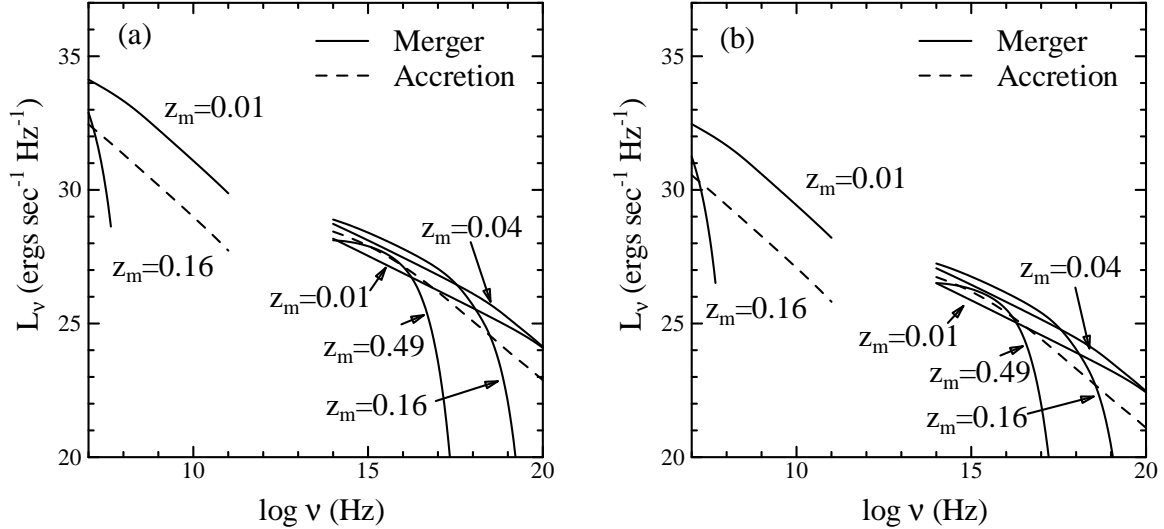


Fig. 10.— Spectra of total emission of a merging or merged cluster for (a) model L1 and (b) model L2. The emission at  $\nu < 10^{11}$  Hz is synchrotron emission and the emission at  $\nu > 10^{14}$  Hz is IC emission. The redshifts indicated in the figure are that at which the cluster merger starts ( $z_m$ ). For comparison, the spectra of total emission from a cluster undergoing accretion is also shown (Figure 6).

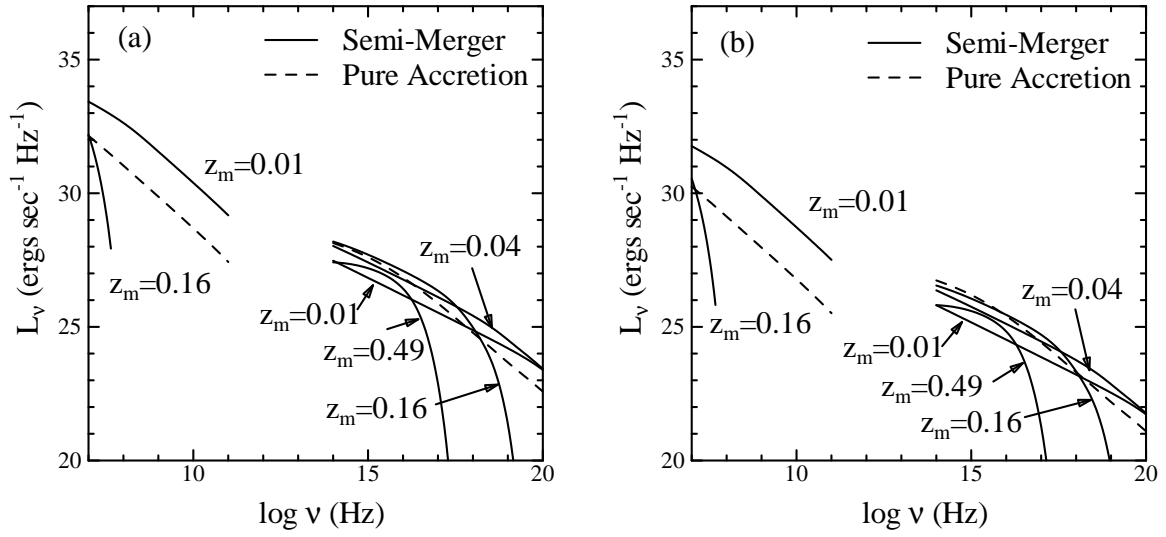


Fig. 11.— The same as Figure 10 but for semi-mergers and pure accretion. (a) model L1 and (b) model L2.

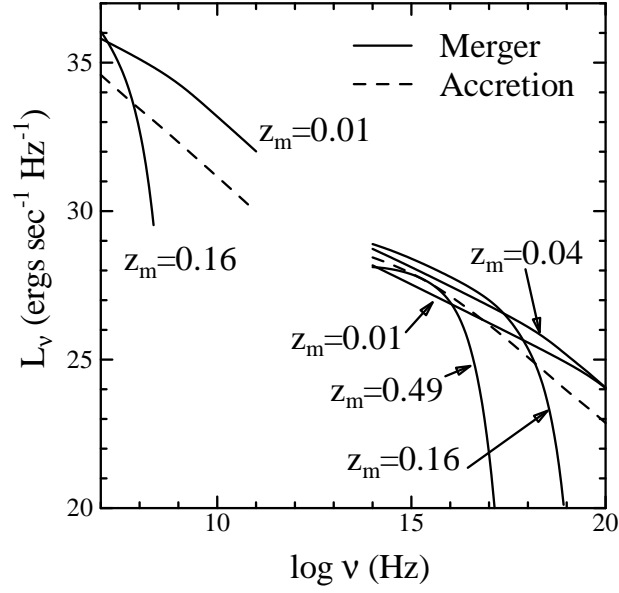


Fig. 12.— The same as Figure 10a except for  $B_0 = 0.1 \mu\text{G}$  (model L1').

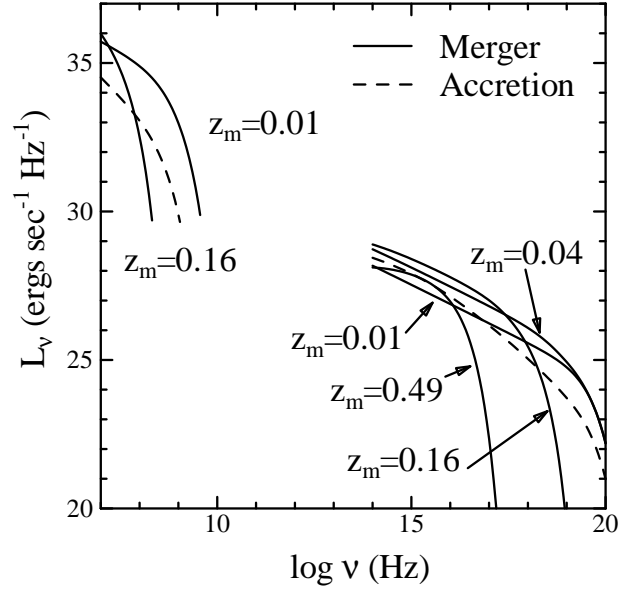


Fig. 13.— The same as Figure 12 except that the initial electron energy distribution has a high-energy cutoff for  $\gamma_i > 10^4$ .



Table 1. Model Parameters.

Models	$\Omega_0$	$\lambda$	$h$	$\sigma_8$	$M_0$	$B_0$
L1	0.3	0.7	0.7	1.00	$10^{15} M_\odot$	$0.01 \mu\text{G}$
L1'	0.3	0.7	0.7	1.00	$10^{15} M_\odot$	$0.10 \mu\text{G}$
L2	0.3	0.7	0.7	1.00	$10^{14} M_\odot$	$0.01 \mu\text{G}$
S1	1.0	0.0	0.5	0.63	$10^{15} M_\odot$	$0.01 \mu\text{G}$
S2	1.0	0.0	0.5	0.63	$10^{14} M_\odot$	$0.01 \mu\text{G}$

Table 2. Merger Fractions in Clusters

Models	$f_{\text{mer}}^{\text{a}}$	$f_{\text{mer,EUV}}^{\text{b}}$	$z_f^{\text{c}}$	$z_{\text{EUV}}^{\text{d}}$	$f_{\text{smer}}^{\text{e}}$
L1	0.09	0.3	0.66	0.4	0.31
L2	0.05	0.2	1.10	0.4	0.21
S1	0.14	0.4	0.36	0.3	0.44
S2	0.07	0.2	0.77	0.3	0.30

<sup>a</sup>Fraction of clusters in a merging phase at  $z = 0$ .

<sup>b</sup>Fraction of the clusters whose EUV luminosities attributed to their last merger is larger than those attributed to accretion at  $z = 0$ .

<sup>c</sup>Average redshift of cluster formation.

<sup>d</sup>Equal EUV redshift (see text)

<sup>e</sup>Fraction of clusters in a semi-merging or merging phase at  $z = 0$ .